Available online at www.sciencedirect.com
ScienceDirect
Nuclear Instruments and Methods in Physics Research B 255 (2007) 114–119
NIM B
Beam Interactions with Materials & Atoms
www.elsevier.com/locate/nimb

Electrical effects of transient neutron irradiation of silicon devices

H.P. Hjalmarson [a,*], R.L. Pease [b], R.M. Van Ginhoven [a], P.A. Schultz [a], N.A. Modine [a]

[a] Sandia National Labs, MS1322, P.O. Box 5800, Albuquerque, NM 87185, United States
[b] RLP Research, Los Lunas, NM 87031, United States

Available online 31 January 2007

Abstract

The key effects of combined transient neutron and ionizing radiation on silicon diodes and bipolar junctions transistors are described. The results show that interstitial defect reactions dominate the annealing effects in the first stage of annealing for certain devices. Furthermore, the results show that oxide trapped charge can influence the effects of bulk silicon displacement damage for particular devices.

PACS: 61.80.Az; 61.82.Ms

Keywords: Silicon; Silicon dioxide; Neutron irradiation; Ionizing radiation; Diodes; Interstitials; Vacancies; Interface traps

1. Introduction

Neutron and ionizing irradiation of bipolar transistors generally causes damage to these devices [1]. Neutron irradiation generates defects by displacing silicon atoms. For each displacement collision, a pair of defects is created, the interstitial atom and the vacancy left behind. These defects reduce transistor gain by increasing the recombination rate of electrons and holes thereby increasing the base current of these devices. After the radiation ceases, these defects undergo reactions that produce composite defects that are less effective at carrier recombination. Ionizing radiation, which occurs during neutron irradiation, also damages these devices, primarily by releasing electrons and holes in the ever-present silicon dioxide in these devices [2]. This process leads to trapped positive charge in the oxide, and it also produces interface traps, often by releasing hydrogen from sites in the oxide. Furthermore, the electric field caused by the trapped charge affects the recombination rate.

A primary motivation for these calculations is the need to understand the expected phenomena from radiation sources that produce varying degrees of atomic displacement effects compared with ionization effects. For example, ion implantation can be used to mimic neutron irradiation but it will be accompanied by larger ionization effects. For this reason, in the simulations to be described, the ionization effects are comparable with the atomic displacement effects.

In this article, we discuss continuum simulations of the temporal evolution of these phenomena, and these simulations rely on information from atomistic simulations of defects in silicon and silicon dioxide. For the displacement defects, density-functional theory (DFT) calculations are used to obtain the energy levels of the defects, primarily interstitials and vacancies. The continuum simulations also use information from DFT and kinetic Monte Carlo atomistic simulations of athermal migration of interstitials driven by carrier injection. Finally, these continuum simulations are used to describe the transient electrical effects of these devices during and after irradiation.

The simulations are used to illustrate some of the consequences of the combined phenomena but they are not used to understand specific data in this report. In these continuum simulations, the sequence of events are described by focusing on three specific phenomena. The first is the response of a diode to combined transient neutron and

* Corresponding author. Tel.: +1 505 844 8888; fax: +1 505 845 7442.
E-mail address: hphjalm@sandia.gov (H.P. Hjalmarson).

0168-583X/$ - see front matter
doi:10.1016/j.nimb.2006.11.123

ionizing radiation. The second is the phenomena in the silicon dioxide portion of this diode. The third is a discussion of the effect of the trapped charge in the oxide on the neutron displacement damage in a diode. In each of these simulations, the radiation dose rates and pulse durations are given values that should be representative of actual values expected if this simulation capability were used for comparisons with experimental data.

2. Simulations

The calculations are performed with REOS (radiation effects in oxides and semiconductors), software developed to solve for the radiation effects response of the silicon semiconductor and its oxide [3]. In these simulations, kinetic equations are solved to obtain the time-dependent effects of ionizing radiation [3–6]. These equations include contributions from the drift–diffusion transport of the mobile species such as electrons, holes, interstitials, vacancies, hydrogen and other atomic species [3,6]. The equations also include contributions from the reactions governing the release of protons and neutral hydrogen from source sites and the reactions of these hydrogen atoms with the silicon dangling bonds at the interface [3,6]. The effects of the electric field are included in these calculations [3–5]. This field includes contributions from the gate bias, the space-charge of all the charged species and the band-bending in the silicon substrate. All the simulations to be discussed are done using REOS.

The simulations to be described focus on the electrical behavior of a uniformly doped silicon diode. This diode consists of a 10-μm thick p-doped region doped with $10^{15}\,cm^{-3}$ boron acceptors, and a 10-μm thick n-doped region doped with $10^{17}\,cm^{-3}$ phosphorus donors. For these one-dimensional simulations, the electrical phenomena are controlled by the more lightly doped region, the p-doped portion. For the two-dimensional simulations including oxide effects, a 1-μm thick portion of this structure is covered by a 1-μm thick layer of silicon dioxide. In agreement with typical samples, a large concentration of interstitial oxygen impurities is also assumed; to be specific, $[O] = 10^{18}\,cm^{-3}$. The initial interstitials and vacancies are allowed to react with each other, with the boron acceptors and with the oxygen impurities. All defects known to create energy levels within the silicon bandgap are allowed to capture and release electrons and holes. The defect reactions are assumed to be diffusion-limited, and the reaction rates are therefore defined in terms of diffusion coefficients and the capture radius for each reaction. The carrier capture and emission reaction rates are obtained from literature values for energy levels and approximations for capture cross-sections. For comparison with the electrical measurements of recombination rates, the interstitials and vacancies are allowed to react with dopants and impurities while electrons and holes were injected.

Numerous simulations were done to explore the defect reactions that control early-time recombination rate annealing. Based on insight gathered from these test calculations, the essence of the early-time annealing can be understood by considering the reactions of interstitials and vacancies with dopants and impurities. Such reactions are more important than direct recombination of interstitials and vacancies unless the irradiation dose is extremely large or one is considering phenomena within a highly defective disordered region.

2.1. Transient annealing

To be specific, this report discusses the few defect reactions that are likely to be important to understand the early-time annealing. The primary reactions are those that remove the main defects, interstitials and vacancies. In the simulations to be described, the following two reactions are the primary reactions:

$$O_i + V \rightarrow O_v$$

and

$$B_s + I \rightarrow B_i.$$

In the first reaction, a vacancy V reacts with interstitial oxygen O_i to create an oxygen–vacancy pair O_v; in the second reaction, an interstitial I reacts with substitutional boron B to create interstitial boron B_i.

When possible, the reaction coefficients are obtained from experimental data. In some cases, no information is available and thus the information was obtained by simple approximations to the atomistic phenomena. In particular, the reaction coefficients for the reactions involving vacancies was obtained by simulating experiments that involved measuring the ESR signal before and after a series of thermal annealing steps [7].

The properties of interstitials are not well known. Similar to vacancies, they are thought to have several charge states in the silicon bandgap. However, these assignments are based on calculations because electrical properties of interstitials have never been measured directly. It is assumed that these defect migrate rapidly and react with other defects.

The rapid migration of interstitials at low temperatures has led to the hypothesis that they migrate via an athermal mechanism driven by sequential recombination of electrons and holes [8,9]. The athermal diffusion occurs because the minimum energy site depends on the charge state of the interstitial, and the hopping of the interstitial from site to site causes diffusive motion [9]. Following the initial proposal, several electronic structure calculations have been undertaken to understand the atomistic details [10–14]. These calculations for interstitials in silicon have concluded that the diffusion involves jumps between the hexagonal and tetrahedral interstitial sites. Some calculations have concluded that the jumps involve the $m = 0$, 1 and 2 charge states but most recent calculations conclude that the jumps involve the $m = 0$ and 1 charge states.

In our implementation of the Recombination Enhanced Diffusion (RED) mechanism, we developed a simplified

continuum model for the underlying atomistic phenomena. We assume transitions between the $m = 0$ (hexagonal) and 1 (tetrahedral) charge states (in this paper we ignore other interesting atomistic effects) [14,15]. To be specific, we assume that each change in charge state leads to an interstitial jump to the appropriate site (at very high rates one might expect that not all transitions produce a jump to another site but we ignore this possibility). Furthermore, we make a conceptual separation between the electronic and nuclear motion of the interstitial; in contrast, earlier atomistic treatments have considered the combined electronic and nuclear dynamics during the transistion [16].

Our continuum mechanism produces the simple expression,

$$D_{\mathrm{RED}} = a^2 r_{\mathrm{m}}, \tag{1}$$

for the RED contribution to the diffusion coefficient; this is the classic expression for a diffusion coefficient in terms of atomistic quantities. In this expression, the jump distance $a = 0.5$ nm is the total distance involved in diffusive motion, and the rate r_{m} is the minimum of the electron and hole capture rates. In other words, the interstitial is assumed to make two atomistic jumps for each diffusive jump and the rate of the slowest jump determines the diffusion coefficient. The recombination rates are obtained by computing the rate of electron and hole recombination in terms of electron and hole cross-sections for the interstitial $m = 0$ and 1 charge states.

It is well known that the neutron irradiation also generates other defects in addition to interstitials and vacancies during the primary displacement events [1]. The most studied and important of these defect species is a divacancy [17]. For these simulations, we assume that 10% of the vacancies form divacancies [18,17].

The values of physical parameters used for the simulations are shown in the tables. Tables 1 and 2 show the information for the vacancies and interstitials, respectively. For these defects, the diffusion prefactors are 10^{-4} cm^2 s^{-1} in all cases. Table 3 shows the information for the other defects. Table 4 shows the information for the carrier recombination reactions and Table 5 shows the information for the defect reactions.

The carrier recombination reactions are assumed to be written in terms of the cross-section associated with each reaction. For example, for the reaction

$$\mathrm{V}^0 + n \rightleftharpoons \mathrm{V}^-,$$

Table 1
Vacancy information

Name	Energy (eV)	Act. energy (eV)
$\mathrm{V}^{=}$	$E_c - 0.09$	0.18
V^{-}	$E_c - 0.4$	0.22
V^{0}	$E_v + 0.05$	0.33
V^{+}	$E_v + 0.13$	0.33
V^{++}		0.33

Table 2
Interstitial information

Name	Energy (eV)	Act. energy (eV)
$\mathrm{I}^{=}$		0.35
I^{-}	$E_c - 0.39$	0.30
I^{0}	$E_v + 0.4$	0.18
I^{+}		0.48
I^{++}		1.17

This information is supplemented by an athermal diffusion model within REOS.

Table 3
Divacancy, A-center and boron-interstitial information

Defect	Name	Energy (eV)
Divacancy	$\mathrm{V}_2^{=}$	$E_c - 0.23$
	V_2^{-}	$E_c - 0.39$
	V_2^{0}	$E_v + 0.21$
	V_2^{+}	
A-center	OV^{-}	$E_c - 0.17$
	OV^{0}	
Boron-interstitial	B_i^{-}	$E_c - 0.45$
	B_i^{0}	$E_c - 0.12$
	B_i^{+}	

Table 4
Carrier recombination reactions for vacancies

Number	Reaction	σ (cm^{-2})	E_f (eV)	E_r (eV)
1	$\mathrm{V}^{++} + \mathrm{n} \rightleftharpoons \mathrm{V}^{+}$	1.0×10^{-13}	0.0	−0.97
2	$\mathrm{V}^{+} + \mathrm{p} \rightleftharpoons \mathrm{V}^{++}$	1.0×10^{-19}	0.0	−1.13
3	$\mathrm{V}^{+} + \mathrm{n} \rightleftharpoons \mathrm{V}^{0}$	1.0×10^{-13}	0.0	−1.05
4	$\mathrm{V}^{0} + \mathrm{p} \rightleftharpoons \mathrm{V}^{+}$	1.0×10^{-16}	0.0	−0.05
5	$\mathrm{V}^{0} + \mathrm{n} \rightleftharpoons \mathrm{V}^{-}$	1.0×10^{-16}	0.0	−0.4
6	$\mathrm{V}^{-} + \mathrm{p} \rightleftharpoons \mathrm{V}^{0}$	1.0×10^{-13}	0.0	−0.7
7	$\mathrm{V}^{-} + \mathrm{n} \rightleftharpoons \mathrm{V}^{--}$	1.0×10^{-19}	0.0	−0.09
8	$\mathrm{V}^{--} + \mathrm{p} \rightleftharpoons \mathrm{V}^{-}$	1.0×10^{-13}	0.0	−1.01

Table 5
Defect reactions

Number	Reaction	k_{f0}
1	$\mathrm{B}_s^{-} + \mathrm{I}^{+} \rightleftharpoons \mathrm{B}_i^{0}$	$4\pi R_0(D_{\mathrm{B}_s^-} + D_{\mathrm{I}^+})$
2	$\mathrm{O}_i^{0} + \mathrm{V}^{0} \rightleftharpoons \mathrm{OV}^{0}$	$4\pi R_0(D_{\mathrm{O}_i^0} + D_{\mathrm{V}^0})$
3	$\mathrm{O}_i^{0} + \mathrm{V}^{-} \rightleftharpoons \mathrm{OV}^{-}$	$4\pi R_0(D_{\mathrm{O}_i^-} + D_{\mathrm{V}^0})$

The activation energies and reverse reaction rates are set to zero.

the forward and reverse reaction rates are:

$$k_{\mathrm{f}} = v_{\mathrm{n}}\sigma \exp(E_{\mathrm{f}}/k_{\mathrm{B}}T), \tag{2}$$

$$k_{\mathrm{r}} = v_{\mathrm{n}}\sigma N_{\mathrm{c}} \exp(E_{\mathrm{r}}/k_{\mathrm{B}}T) \tag{3}$$

in which v_{n} is the thermal velocity for electrons, σ is the cross-section, and N_{c} is the thermal density of states for the conduction band. A similar expression can be written for the reactions involving holes in terms of v_{p}, the thermal velocity for holes, and N_{v}, the thermal density of states for the valence band.

3. Results and discussion

The results to be shown focus on the combined effects of radiation on room temperature carrier recombination in a silicon diode. The focus is on early time phenomena in the transient annealing immediately after a radiation pulse. The primary initial species are assumed to be interstitials, vacancies, divacancies, electrons and holes.

3.1. Transient annealing

In these simulations, the vacancies react with oxygen interstitial defects, the interstitials react with the acceptor dopants, and the divacancies do not undergo reactions. In addition, these simulations include an athermal diffusion mechanism for the interstitials.

The first calculation focuses on transient neutron irradiation of a simple diode previously described. For these simulations, the radiation consists of uniform pulses. These pulses generate interstitials and vacancies at a rate $G_{IV} = 10^{22}\,cm^{-3}\,s^{-1}$, divacancies at a rate $G_{VV} = 10^{21}\,cm^{-3}\,s^{-1}$, and electrons and holes at a rate $G_{np} = 10^{22}\,cm^{-3}\,s^{-1}$. These spatially-uniform pulses have a time duration of 10^{-8} s.

The calculations focused on the effects of this irradiation on the forward current of a diode for two bias conditions, $V_{low} = 0.4$ V and $V_{high} = 0.5$ V. The electrical current through the diode is shown as a function of time in Fig. 1.

Initially this current is positive because the diode is forward biased in both cases. Due to the injected carriers, the current reverses and this negative photocurrent begins to rise (open symbols). For the lowest bias, the photocurrent reaches a steady state value, and then it begins to decrease due to the injected defects. The higher bias current, however, shows no steady state value before it begins to decrease. These effects on the photocurrent are caused by the increased carrier recombination by the increasing density of injected defects, primarily the interstitials. These defects reduce the diffusion length, a fundamental physical parameter governing the portion of the diode from which carriers are collected. Effectively this reduces the volume from which photocurrent is collected thereby reducing the photocurrent. This reduction in the diffusion length also increases the forward current in the diode. The net effect of these combined effects is to reduce the magnitude of the photocurrent prior to the end of the pulse.

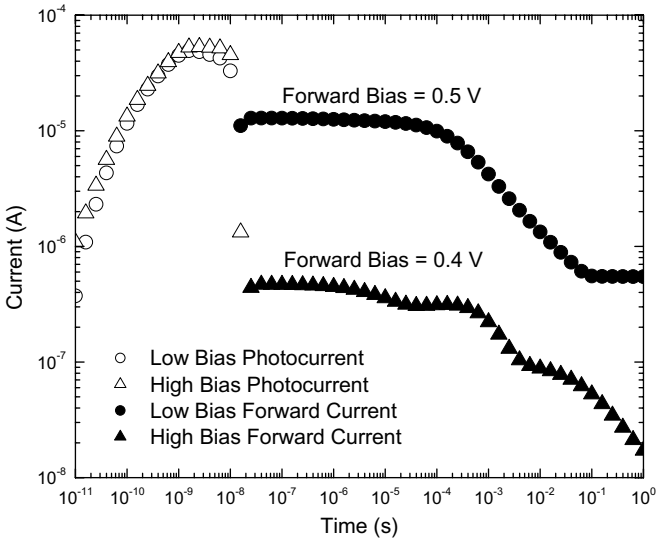

Fig. 1. The diode current as a function of time following transient neutron irradiation for low and high bias. The results show the negative photocurrent (open symbols) and the positive forward current (closed symbols). At long times the forward currents approach their values prior to irradiation because much of the radiation damage has been annealed. These annealing phenomena are discussed in the body of this report.

Immediately after the pulse ceases, the forward current of the diode dominates (closed symbols). In both cases, this current becomes smaller due to annealing of the defects. When the pulse ends, the photocurrent drops rapidly, governed by the recombination rate determined by the injected interstitials and vacancies.

The lowest bias current shows two distinct annealing regions. In the first region, the dominant effect is annealing of the vacancies. When this annealing ceases, annealing of the interstitials continues to reduce the current.

For the higher bias, the vacancy annealing region is absent because vacancy–carrier recombination is less effective at the increased carrier density associated with this higher bias. Furthermore, the interstitial annealing is faster due to the larger density of injected electrons. At longer times the forward current is governed by the annealed species and the injected divacancies whose annealing is not included in these calculations focused on the first stage of annealing.

Consideration of the details of the calculations for higher bias reveals two other phenomena that affect the vacancy contribution to the annealing. One phenomenon is the increased fraction of negative vacancies due to injection of electrons. Given the larger diffusion coefficients of the negative vacancies, the electron injection thus leads to faster annealing. However, this effect is relatively small for these room temperature calculations. The other phenomenon that reduces the annealing contribution by vacancies is the saturation of the carrier recombination rate when the carrier density is high. The end result is that the net rate is governed by the slowest of the vacancy capture rates.

At other injection rates for samples that are more lightly doped, the injected carrier density may become large enough that the charge state dependence of vacancy diffusion rates will become a factor that governs the time-dependence of the annealing factor. However, in the simulations whose results are shown here, the dopant density is large enough that most of the vacancies are neutral unless the carrier injection is very large.

In summary, the main contribution to the recombination rate at short times is due to interstitial recombination. The evolution to shorter times with increasing carrier injection is due to the increased athermal diffusion stimulated

by the carrier recombination at the interstitials. The timescale of vacancy evolution is nearly independent of injection rate. At the highest injection level, substantial interstitial annealing occurs before vacancy annealing. Thus the vacancy contribution shows up as a plateau in that simulation.

These results show the same trends with injection level and temperature as seen in the early data [19–21]. The physics explanation found in these simulations differs from that suggested by the early studies. In these studies, it was inferred that the annealing rate was governed by vacancies and that differing effects arose through the differing diffusion coefficients for the various charge states [20].

3.2. Oxide effects

The photocurrent collected in the oxide can have dramatic consequences on the behavior of a bipolar transistor. These effects are especially large for an NPN transistor. For this case, the trapped charge in the oxide produces band-bending that increases the carrier recombination rate near the base–emitter junction of a transistor. In many cases, this effect can dominate other contributions to the base current.

Furthermore, the ionizing radiation generally creates interface traps. The mechanism likely involves the release of hydrogen in the oxide. This hydrogen migrates to the interface where it creates interface traps by de-passivating an existing hydrogen-passivated interface trap. The timescale for the creation of these traps appears to depend on the location of the hydrogen source sites.

To illustrate the oxide effects, the electrical behavior of a gate diode is simulated. This diode structure has a 1-μm thick oxide layer between the 1-μm thick silicon diode (described in the previous section) and another silicon layer, the heavily doped gate. The 1-μm thick gate has 10^{18} cm^{-3} n-type doping. The gate bias is varied to simulate the effect of trapped charge in the oxide.

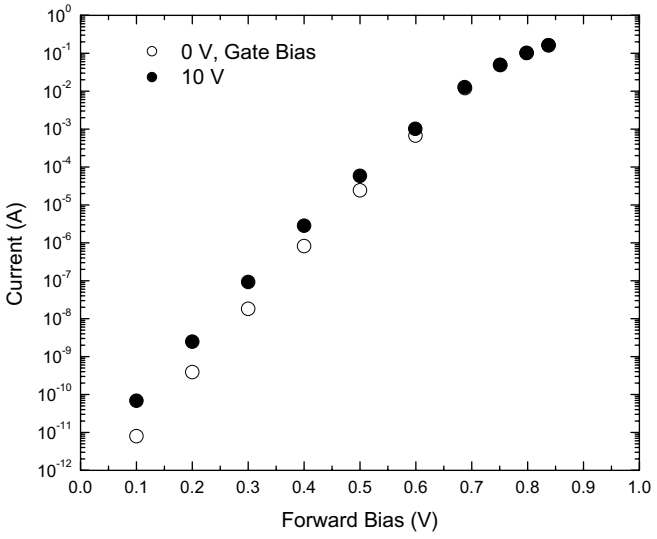

Fig. 2. The gated-diode current as a function of forward bias for no gate bias and 10 V gate bias. The gate bias simulates the effects of trapped charge from the ionizing radiation. As shown in this figure, the trapped charge accentuates the effects of the carrier recombination defects created by the neutrons.

Fig. 2 shows the forward diode current as a function of gate bias for two different gate potentials, $V_G = 0$ and $V_G = 10$ V. The results show that the gate bias has its most dramatic effect at low forward bias.

The gate bias acts primarily to reduce the hole density near the interface. As a consequence, the injected electron current is increased. This leads to a more conductive region near the interface. However, as the forward bias increases, the remaining portion of the diode contributes more and more to the current. As a result, the effect of the gate bias is lessened.

An important observation is that this enhancement has been computed for a uniform trap density. The enhancement may become larger if interface traps are also created by the radiation but this possibility is not considered in this report.

4. Conclusions

In summary, these calculations reveal that the essence of transient neutron annealing at short times in p-type silicon can be simulated by considering two first-stage defect reactions, one for vacancies and one for interstitials. The injection dependence of the simulations is similar to that seen in data. Furthermore, these calculations have shown that the effect of ionizing radiation is to increase the current in a diode. A consequence of this effect for a transistor is a reduction in gain due to trapped charge in the oxide.

In future work, similar simulations that combine these physical mechanisms can be used to determine the effects of these combined phenomena for various radiation sources.

Acknowledgment

Sandia is a multiprogram laboratory operated by Sandia Corporation, a Lockheed Martin Company, for the United States Department of Energy's National Nuclear Security Administration under Contract DE-AC04-94AL85000.

References

[1] J.R. Srour, C.J. Marshall, P.W. Marshall, IEEE Trans. Nucl. Sci. 50 (2003) 653.
[2] T.P. Ma, P.V. Dressendorfer (Eds.), Ionizing Radiation Effects in MOS Devices and Circuits, John Wiley and Sons, New York, NY, 1989.
[3] H.P. Hjalmarson, R.L. Pease, S.C. Witczak, M.R. Shaneyfelt, J.R. Schwank, A.H. Edwards, C.E. Hembree, T.R. Mattsson, IEEE Trans. Nucl. Sci. 50 (2003) 1901.
[4] V. Vasudevan, J. Vasi, J. Appl. Phys. 70 (1991) 4490.
[5] R. Sokel, R.C. Hughes, J. Appl. Phys. 53 (1982) 7414.
[6] S.N. Rashkeev, C.R. Cirba, D.M. Fleetwood, R.D. Schrimpf, S.C. Witczak, A. Michez, S.T. Pantelides, IEEE Trans. Nucl. Sci. 49 (2002) 2650.

[7] G.D. Watkins, in: F.A. Huntley (Ed.), Lattice Defects in Semiconductors, 1974, Institute of Physics, London, 1975, p. 1.
[8] G.D. Watkins, J. Phys. Soc. Japan 18 (1963) 22.
[9] J.C. Bourgoin, J.W. Corbett, 38A (1972) 135.
[10] Y. Bar-Yam, J.D. Joannopoulos, Phys. Rev. B 30 (1984) 2216.
[11] G.D. Watkins, Phys. Rev. B 12 (1975) 5824.
[12] J.R. Troxell, A.P. Chatterjee, G.D. Watkins, Phys. Rev. B 19 (1979) 5336.
[13] P.E. Blöchl, E. Smargiassi, R. Car, D.B. Lake, W. Andreoni, S.T. Pantelides, Phys. Rev. Lett. 70 (1993) 2435.
[14] W.C. Lee, S.G. Lee, K.J. Chang, J. Phys.: Condens. Matter 10 (1998) 995.
[15] N.A. Modine, unpublished.
[16] W.A. Harrison, Phys. Rev. B 57 (1998) 9727.
[17] J.W. Corbett, G.D. Watkins, Phys. Rev. 138 (1965) A555.
[18] G. Davies, E.C. Lightowlers, R.C. Newman, A.S. Oates, Semicond. Sci. Technol. 2 (1987) 524.
[19] B.L. Gregory, H.H. Sander, IEEE Trans. Nucl. Sci. 14 (1967) 116.
[20] B.L. Gregory, H.H. Sander, Proc. IEEE 58 (1970) 1328.
[21] H.P. Hjalmarson, unpublished.